THE JOURNAL OF PHYSICAL CHEMISTRY A

Article

Cite This: J. Phys. Chem. A 2019, 123, 862−872

pubs.acs.org/JPCA

Conformational Preferences of Isolated Glycylglycine (Gly-Gly) Investigated with IRMPD-VUV Action Spectroscopy and Advanced Computational Approaches

Vasyl Yatsyna,[†,‡] Ranim Mallat,[†] Tim Gorn,[§] Michael Schmitt,[§] Raimund Feifel,[†] Anouk M. Rijs,*[,‡] and Vitali Zhaunerchyk*[,†]

[†]Department of Physics, University of Gothenburg, 412 96 Gothenburg, Sweden

[‡]Radboud University, Institute of Molecules and Materials, FELIX Laboratory, Toernooveld 7-c, 6525 ED Nijmegen, The Netherlands

[§]Institut für Physikalische Chemie I, Heinrich-Heine-Universität, D-40225 Düsseldorf, Germany

Supporting Information

ABSTRACT: In this article, we report the results of gas-phase IR spectroscopy of neutral glycylglycine (Gly-Gly) in the 700−1850 cm^{-1} frequency range. A combination of laser desorption, jet-cooling, and IR multiple-photon dissociation vacuum−ultraviolet (IRMPD-VUV) action spectroscopy is employed, together with extensive quantum chemical calculations that assist in the analysis of the experimental data. As a result, we determined that the most favorable conformer in the low-temperature environment of the supersonic jet is the nearly planar structure with two C5 hydrogen-bonding interactions. Calculations clearly show that this conformer is favored because of its flexibility (considerable entropy stabilization) as well as efficient conformer relaxation processes in the jet. To gain more understanding into the relative stability of the lowest-energy Gly-Gly conformers, the relative strength of hydrogen bonding and steric interactions is analyzed using the noncovalent interactions (NCI) approach.

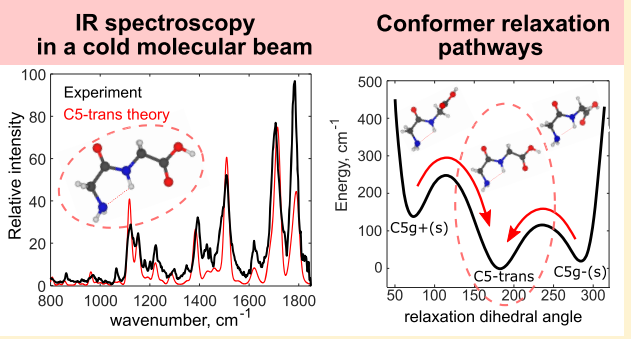

1. INTRODUCTION

Gas-phase infrared (IR) spectroscopy of small and medium peptides[1−8] allows insight into protein folding forces[9−12] at the atomic level. Thanks to the development of various techniques to transfer intact biomolecules into the gas phase, IR spectroscopy became a routine tool for studies of biomolecular systems of increasing size and complexity.[13] It has the advantage of a high sensitivity of molecular vibrations to the backbone structure and noncovalent interactions such as hydrogen bonding.

Because low sample density in the gas phase restricts direct IR absorption measurements, action spectroscopy techniques are employed instead. In action spectroscopy, the IR photon absorption is detected through a change in the ionization or fluorescence yield, electron detachment, or fragmentation.[14] Double-resonance IR-UV spectroscopy is a powerful method that allows the recording of IR spectra of individual molecular conformers. This method, however, can be applied only to molecules with an aromatic UV chromophore. Among the 20 standard amino acids, only three have such a UV chromophore, which significantly limits the scope of the peptides which can be studied. For the spectroscopy of charged species, several techniques are available, such as tagging ("messenger") technique and IR multiple-photon dissociation (IRMPD), whereas IR spectroscopy of neutral isolated peptides without an aromatic ring remains challenging. One way to circumvent this problem is to attach an aromatic moiety, either chemically[15] or through noncovalent interactions.[16] While this approach has found wide application, the attached aromatic group can modify the intrinsic properties of the peptide by introducing extra noncovalent interactions which may also alter its conformational landscape.

Recently, we have demonstrated that the combination of IRMPD spectroscopy of a molecular beam with single-photon vacuum−ultraviolet (VUV) ionization can be used to record the vibrational spectra of cooled neutral molecules of arbitrary structure, without an aromatic chromophore in particular.[17] In the current work, we apply this approach to IR spectroscopy of chromophore-free glycyl-glycine (Gly-Gly). An initial challenge in obtaining gas-phase vibrational spectra for Gly-Gly and other thermolabile molecules is how to volatilize an intact molecule. For the studies of charged Gly-Gly species, electrospray ionization methods were employed, yielding protonated or deprotonated molecular targets.[18−22] In this

Received: November 8, 2018
Revised: January 2, 2019
Published: January 4, 2019

DOI: 10.1021/acs.jpca.8b10881
J. Phys. Chem. A 2019, 123, 862−872

case, however, one has to disentangle the effects of the proton on the peptide's intrinsic structural properties from its vibrational signatures. The laser ablation method is commonly used for the rotational spectroscopy of neutral thermolabile molecules, though in many cases its application to peptides and amino acids is associated with significant photofragmentation effects.[23−25] Only recently has a rotational spectroscopy study of laser-ablated Gly-Gly been reported.[26] In our work, we employ a soft laser desorption process, which imparts minimal internal energy to the desorbed molecules,[14,27] followed by collisional cooling in an argon supersonic jet.

The purpose of the current work is threefold. First, we aim to obtain the IR signatures of the ensemble of Gly-Gly conformers populated under our experimental conditions and compare them to theoretical calculations in order to identify the most abundant conformers. Although the recent rotational spectroscopy study of Gly-Gly observed three different conformers,[26] their abundances were not reported. This leaves some open questions, for instance, about the relative stability of the observed folded and planar structures, especially in view of favorable entropic stabilization[28,29] in the latter. In this respect, the current work will complement the previous rotational spectroscopy results.[26] Second, by studying Gly-Gly we intend to explore the use of the IRMPD-VUV approach for structural analysis of flexible peptides with a large degree of conformational heterogeneity. Third, we aim to shed some light on the strength and importance of noncovalent interactions that are present in the Gly-Gly conformers. For this purpose, we will employ electron density topological analysis within atoms in molecules (AIM)[30−32] and noncovalent interaction (NCI) approaches.[33−35]

2. METHODS

2.1. Experiment and Data Analysis. The experiments were performed at the free electron laser FELIX Laboratory at Radboud University, Nijmegen, The Netherlands, using the laser desorption molecular beam setup.[14] A Gly-Gly sample was obtained commercially from Sigma-Aldrich (purity of 98%). The sample was mixed with carbon black and applied to a graphite bar that was placed in front of a pulsed valve nozzle (0.5 mm orifice, Jordan TOF Products, Inc.) in a source vacuum chamber. The sample molecules were laser desorbed from the bar using a Nd:YAG laser (1064 nm, 5 ns, 1−2 mJ/pulse, Polaris II, New Wave Research) and then seeded into a supersonic jet created by a pulsed valve with argon (3 bar) as a carrier gas. The supersonic jet expansion allowed the desorbed molecules to efficiently cool to the rovibrational ground state. The molecules in the central and coldest part of the expansion region were collimated by a skimmer and delivered to the interaction chamber, where the molecular beam was crossed with a pulsed IR beam from the FELIX free electron laser (FEL). The IR frequency of FELIX was scanned in the range of 700−1850 cm^{-1} corresponding to IR pulse energies of 30−80 mJ. The exposure time to the IR FEL radiation within the interaction region is directly proportional to the mass of the carrier gas; the heavier the gas, the longer the exposure time. With a typical FELIX macropulse duration of 6−8 μs, the sample molecules carried by argon had an estimated residence time of 3 μs in the interaction region. If a molecular vibrational transition was resonant with the scanned IR light frequency, then the molecule dissociated via the infrared multiple-photon dissociation (IRMPD) process. At the end of the FELIX macropulse, the IRMPD fragments and parent molecules were ionized by 118 nm VUV laser pulses of ∼2 to 3 ns duration ($h\nu$ = 10.5 eV, ninth harmonic of a Nd^{3+}:YAG laser, Spectra-Physics). The created ions were detected by means of a reflectron-type time-of-flight mass spectrometer. By measuring the IRMPD fragmentation yield versus the FELIX wavelength, the vibrational IRMPD-VUV spectrum of Gly-Gly was obtained. The FELIX laser was operated at 5 Hz, while the desorption laser, the pulsed valve, and the VUV ionizing laser were operated at 10 Hz. This enabled the measurement of reference mass spectra without IR radiation for every second VUV laser pulse (Figure 1).

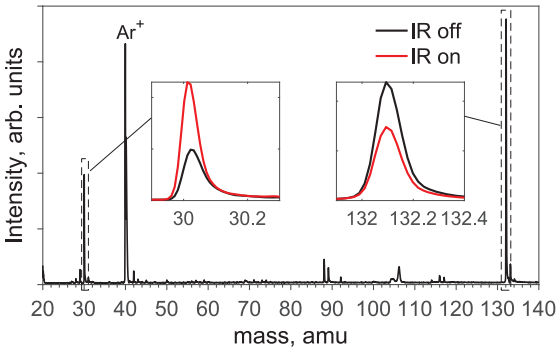

Figure 1. VUV (10.5 eV) mass spectra of laser-desorbed Gly-Gly molecules under IR on (red curve) and IR off (black curve) conditions. The inset plots show how the fragment peak at 30 amu and parent peak at 132 amu change their intensities when the IR FELIX wavelength is resonant with a vibrational transition of Gly-Gly.

The VUV laser light was generated by focusing 355 nm light (third harmonic of Nd^{3+}:YAG laser) into the center of a gas cell containing a 1:10 mixture of Xe and Ar gases. The resulting 118 nm laser beam was refocused into the molecular interaction region through a MgF_2 lens. The residual 355 nm beam remained divergent and was not focused in the interaction region since the focal distance of the MgF_2 lens was larger for 355 nm. To further separate the 118 and 355 nm beams, we used off-axis alignment through the MgF_2 lens. The estimated pulse energy of the generated VUV radiation was ≤1 μJ on the basis of the conversion efficiency of 10^{-4} in the phase-matched Xe−Ar mixture.[36,37]

Assuming a constant interaction volume and a constant time profile of macropulses upon scanning the FELIX wavelength, a relative absorption cross section versus IR frequency can be expressed through the experimentally measured quantities as

$$\sigma_{rel} = \frac{1}{N_{ph}} \ln\left(\frac{P_{off}}{P_{on}}\right) \quad (1)$$

where N_{ph} denotes the number of photons in the IR pulse, P denotes the intensity of the parent ion, and the "on" and "off" subscripts refer to the measurements performed with FELIX being on and off, respectively. If all IRMPD fragments $\sum F_{i,\,on}$ are detected, then the P_{off} signal is equal to $\sum F_{i,\,on} + P_{on}$, and eq 1 can be expressed as

$$\sigma_{rel} = \frac{1}{N_{ph}} \ln\left(\frac{\sum F_{i,on} + P_{on}}{P_{on}}\right) \quad (2)$$

Equation 2 is preferable to eq 1 because it involves only quantities measured with FELIX being on and hence allows the

DOI: 10.1021/acs.jpca.8b10881
J. Phys. Chem. A 2019, 123, 862−872

elimination of shot-to-shot fluctuations of the laser desorption source. To implement eq 2 into the current measurements, it should be corrected for a fraction of fragments produced solely by VUV in the absence of the FELIX pulses. Corrected eq 2 takes the form

$$\sigma_{rel} = \frac{1}{N_{ph}} \ln\left((1-\alpha)\frac{\sum F_{i,on} + P_{on}}{P_{on}}\right) \quad (3)$$

where α denotes the fraction of the parent molecules that undergo fragmentation when the molecules are not irradiated with FELIX. This fraction can be found as

$$\alpha = \frac{\sum F_{i,off}}{\sum F_{i,off} + P_{off}} \quad (4)$$

We note that eq 3 neglects the multiple-photon nature of the IRMPD process. Nevertheless, it is valid for our measurements, assuming that IRMPD signals are observed only when the IR frequency is resonant with a molecular vibration and the IR intensity is sufficiently high to dissociate the molecule.

The Gly-Gly raw spectra were obtained by scanning the FELIX IR laser in the range of 700−1850 cm^{-1} and measuring the relative intensities of the IRMPD fragments and the parent molecule. The final spectrum (Figure 4) was obtained by applying eq 3 to the data and taking into account the FELIX power profile across the measured range. Becauase there were no variations in α (see eq 4) when scanning FELIX, a constant α factor was used in the analysis of each FELIX scan. The mean width of the measured IR bands (fwhm of ∼1.6% of the center frequency) was slightly larger than the bandwidth of the FELIX laser (0.5−1%). This is related to the multiple-photon excitation involved in the IRMPD process that is known to broaden the vibrational transitions.[38]

2.2. Theoretical Treatment. To explore the conformational space of Gly-Gly, a random search method was applied.[39] A large number of structures (∼657 000) with random torsional angles for rotatable bonds was generated and optimized with a semiempirical quantum chemical method, PM6-D3H4,[40] implemented in the MOPAC[41] program package. PM6-D3H4 corrects for dispersion, hydrogen bonding, and the too small hydrogen steric repulsion in genuine PM6. The resulting structures were sorted according to their relative energies, and duplicate structures were discarded. The geometries of obtained unique structures (∼80) with relative energies below 1600 kJ/mol were optimized with higher-accuracy DFT methods using quantum chemistry package *Gaussian 16*.[42] The selection of DFT functionals was based on their performance for similar dipeptide systems.[43] The selected methods (ωB97X-D/6-311++G(d,p),[44] M06-2X/6-31+G(d),[45] MP2/aug-cc-pVTZ, and B3LYP-D3BJ/N07D[46,47]) were further assessed by comparing theoretical predictions with the Gly-Gly experimental rotational constants available elsewhere.[26] (See Table S1 in the Supporting Information). As a result, we have determined that the ωB97X-D functional with the 6-311++G(d,p) basis set is the most reliable for structure calculations of the Gly-Gly peptide.

The lowest-energy Gly-Gly conformers found with our conformational search are shown in Figure 3. Their energies and dihedral angles, denoted in Figure 2, are presented in Table 1. We found that the backbone of most of the conformers deviates from planarity by at least 10°, with one

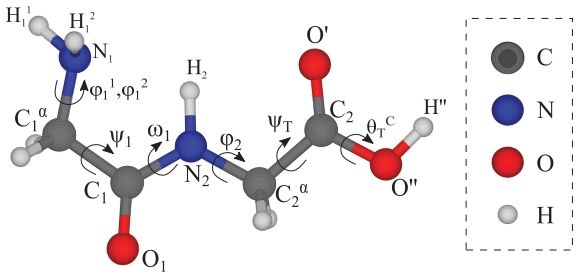

Figure 2. Structure of the Gly-Gly molecule in the cis−trans backbone configuration at the N- and C-termini, respectively (ψ_1 close to 0° and ϕ_2 close to 180°).

exception of the ***sc-cis−trans*** structure that is nearly planar. Moreover, each nonplanar conformer exists as a pair of enantiomeric structures with identical energy. As a result, all structures shown in Figure 3 have a degeneracy factor of 2, except for the planar ***sc-cis−trans*** conformer, which has a degeneracy factor of 1.

For the assignment of the experimental IR bands, the spectra of all low-energy structures of Gly-Gly were calculated. For this purpose, harmonic frequencies and intensities were calculated with the B3LYP-D3BJ functional (Becke, three-parameter Lee−Yang−Parr with D3 version of Grimme's dispersion with Becke-Johnson damping[46]) and the N07D basis set.[47] Anharmonic frequencies and intensities were calculated for the most important low-energy structures using vibrational second-order perturbation theory (VPT2).[48] The B3LYP-D3BJ/N07D method was chosen for both the harmonic and anharmonic frequency calculations because it provides high accuracy within a reasonable computational time.[48−51]

It was shown that the population of conformers upon laser desorption and subsequent supersonic-jet expansion is well reflected by a relative Gibbs free energy distribution at 300−500 K, while the conformational assignments based on electronic energies with zero-point energy (ZPE) corrections should be avoided.[27−29,52−54] To calculate highly accurate Gibbs free energies, we used composite methods CBS-QB3[55] and G4MP2[56] with a modification described in ref 43: high-level single-point energy calculations were based on molecular geometries and frequency calculations obtained using both the ωB97X-D/6-311++G(d,p) and B3LYP-D3BJ/N07D methods. These methods were chosen because they are more reliable for geometry and frequency calculations[43] than the default methods used in CBS-QB3 and G4MP2.

The lowest-energy vibrational modes are known to be poorly described by the harmonic approximation,[57,58] which can have an adverse effect on the accuracy of calculated Gibbs free energies. The treatment of some low-energy torsional vibrations as hindered rotations provides a better description.[59] Therefore, in our analysis we applied an automatic procedure available in Gaussian[59] to identify hindered rotations, and we corrected the calculated free energy using the following relation

$$\Delta G_{vib} = (\Delta E_{vib} + \Delta E_{vib}^{hind}) - T(\Delta S_{vib} + \Delta S_{vib}^{hind})$$

where ΔE_{vib}^{hind} and ΔS_{vib}^{hind} are the hindered rotor approximation corrections[60] to the vibrational thermal energy and entropy, respectively.

For the calculation of relaxation barriers between the conformers, a transitions-state (TS) search was performed

DOI: 10.1021/acs.jpca.8b10881
J. Phys. Chem. A 2019, 123, 862−872

Table 1. Zero-Point-Energy-Corrected G4MP2 Electronic Energies $\Delta(E + ZPE)$, Gibbs Free Energies ΔG at 400 K, and Dihedral Angles of the Lowest-Energy Conformers of Gly-Gly Shown in Figure 3, as Obtained from the ωB97X-D/6-311++G(d,p) Optimized Geometries[a]

	$\Delta(E + ZPE)$, cm^{-1} (kJ/mol)	ΔG at 400 K, cm^{-1} (kJ/mol)	ψ_1	ω_1	ϕ_2	ψ_T	θ_T	ϕ_1^1	ϕ_1^2
C5-trans	0 (0)	0 (0)	−13.2	−179.1	−173.5	−0.9	179.7	150.4	−88.4
C5g-(s)	90 (1.1)	177 (2.1)	−20.1	170.3	−91.8	−2.0	−179.7	156.0	−83.4
C5g+(s)	179 (2.1)	199 (2.4)	−10.5	−169.7	90.3	2.6	179.7	147.9	−91.1
C5C7+	22 (0.26)	485 (5.8)	−10.2	175.9	74.1	123.1	1.0	142.5	−96.1
C5C7−	12.5 (0.15)	474 (5.7)	−11.4	−173.1	−74.6	−122.8	−1.2	144.0	−94.7
trans−trans	408 (4.9)	378 (4.5)	−170.1	−177.5	179.5	−0.1	180.0	−52.4	63.6
C5g-(a)	592 (7.1)	613 (7.3)	−18.0	175.1	−92.6	−176.5	178.5	152.6	−86.9
C5g+(a)	617 (7.4)	809 (9.7)	−11.2	−172.6	89.6	177.6	−178.5	149.4	−89.9
g-trans−trans	664 (7.9)	876 (10.5)	−151.5	−176.8	−179.1	0.5	−179.8	−155.1	−35.3
sc-cis−trans	755 (9.0)	506 (6.1)	−0.01	−180.00	−179.99	0.00	180.00	−64.1	64.1

[a]See Figure 2 for the description of the dihedral angles. Energies are calculated using the G4MP2 method based on the ωB97X-D/6-311++G(d,p) geometries and harmonic frequencies and are presented with respect to the ***C5-trans*** energies in cm^{-1}. Values in kJ/mol are shown in parentheses.

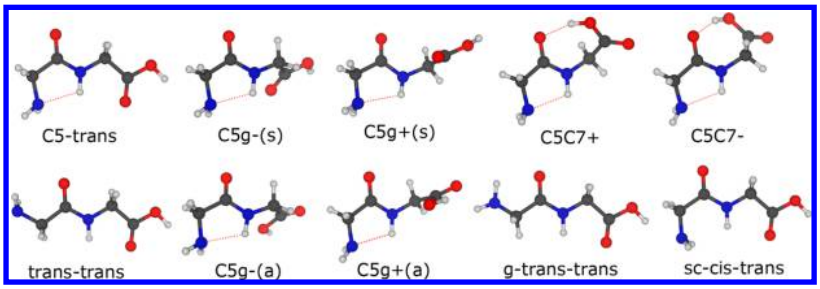

Figure 3. Structures of the lowest-energy conformers of Gly-Gly ($\Delta(E + ZPE)$ below 840 cm^{-1}, 10 kJ/mol) optimized with the ωB97X-D/6-311++G(d,p) method.

using the QST2 and QST3 methods[61] as implemented in *Gaussian*. In the cases where QST2 failed to find a TS, the QST3 method was applied, for which an initial guess of the TS structure was obtained from the relaxed PES scan connecting two conformers. To obtain the barriers to relaxation, accurate electronic and Gibbs free energy calculations were performed by applying the G4MP2 method to the optimized TS structures and the corresponding conformers. Geometry optimization and hindered rotor frequency analysis were performed with the ωB97X-D/6-311++G(d,p) method.

The identification of hydrogen bonding and other weak noncovalent interactions was performed using the electron density $\rho(\mathbf{r})$ topology analysis with the help of *Multiwfn* software.[62] In the first step, the search of bond critical points (BCPs) within the AIM (atoms in molecules)[30] theory was undertaken. BCPs are saddle points in the electron density map $\rho(\mathbf{r})$, representing a minimum in the bonding direction and a maximum in all other directions.[32] Mathematically, this is described by the sign of eigenvalues λ_1, λ_2, λ_3 of the second-order derivative matrix of $\rho(\mathbf{r})$. At BCPs, λ_1 and λ_2 are negative while λ_3 is positive. Ring critical points (RCPs) associated with ring-type structures correspond to second-order saddle points ($\lambda_1 < 0$, λ_2 and $\lambda_3 > 0$).[32] Following AIM analysis, which is useful for the identification of strong hydrogen bonds, we have also applied the NCI (noncovalent interactions) approach.[33] This approach is based on the exploration of NCI index isosurfaces[33] filled with a color map from $\sin(\lambda_2)\rho$ data. The NCI index corresponds to the reduced density gradient (RDG)[33]

$$\mathrm{RDG}(\mathbf{r}) = \frac{1}{2(3\pi^2)^{1/3}} \frac{|\nabla\rho(\mathbf{r})|}{\rho(\mathbf{r})^{4/3}}$$

where $\rho(\mathbf{r})$ is an electron density map that can be obtained from DFT calculations. In our work, we have used the electron density data from the ωB97X-D/6-311++G(d,p) method because this method has been found to provide the best description for Gly-Gly geometries. It is also worth noting that any other DFT or wave-function-based methods with sufficient basis sets are expected to be equally reliable for NCI analysis.[35]

3. RESULTS AND DISCUSSION

3.1. IR Spectroscopy: Experiment, Theory, and Gly-Gly Conformers. The experimental IRMPD spectrum of jet-cooled Gly-Gly is presented in Figure 4 (the black trace in each plot). The IRMPD-VUV method is not conformer-selective, so all conformers sufficiently populated in the molecular beam contributed to the measured spectrum. For comparison, Figure 4 presents the calculated scaled harmonic frequency spectra of several characteristic lowest-energy Gly-Gly conformers (the colored bar spectra). Because vibrational transitions at frequencies below 1100 cm^{-1} have lower intensities, the two different frequency ranges are plotted in panels a and b of Figure 4. Comparison with other conformers that are higher in energy or have similar spectra can be found in Figure S1 of the Supporting Information. It can be seen from Figure 4 that most of the experimental features are readily reproduced by the calculated spectrum of ***C5-trans*** (red bars), which is the lowest-energy conformer. Moreover, the measured spectrum shows considerable differences with the calculated spectra of all other low-energy conformers. (See also Figure S1 in the Supporting Information.) This implies that the measured spectrum is dominated by ***C5-trans***. Such a conclusion is elaborated in more detail in what follows.

DOI: 10.1021/acs.jpca.8b10881
J. Phys. Chem. A 2019, 123, 862−872

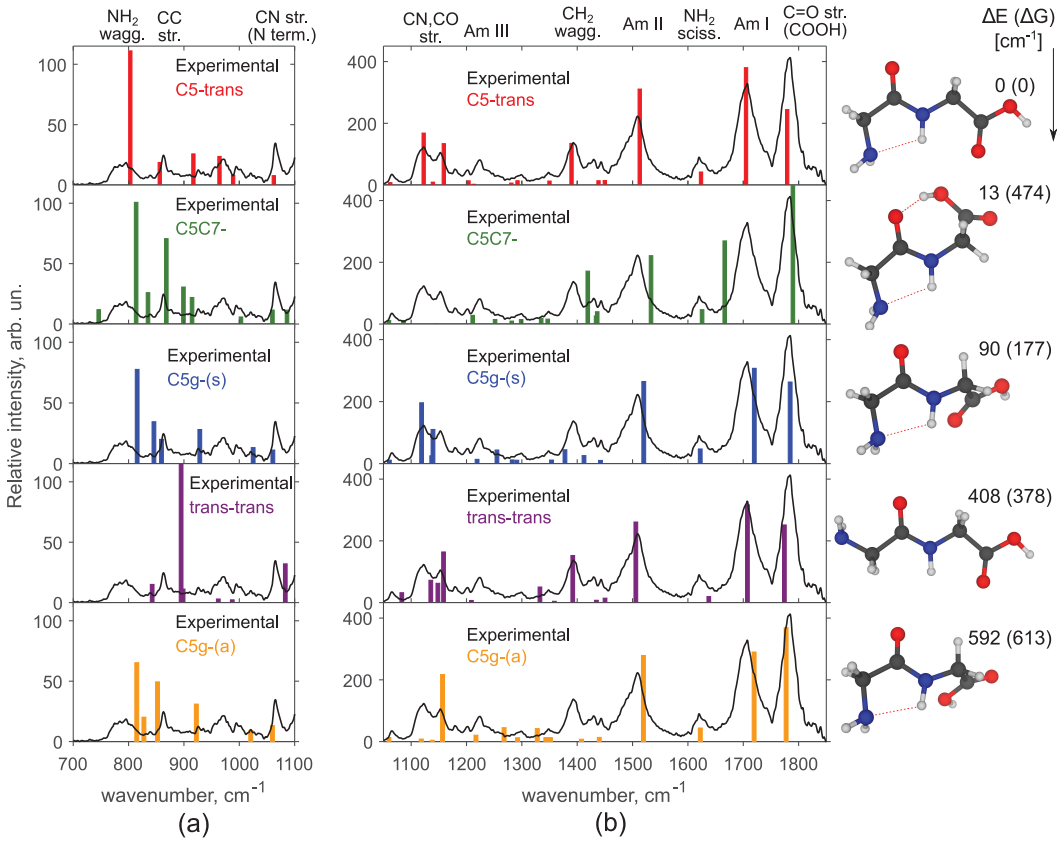

Figure 4. Experimental IRMPD spectra (the black trace in each plot) compared with the scaled harmonic frequency spectra (B3LYP-D3BJ/N07D, scaling factor 0.976) of several of the lowest-energy conformers of Gly-Gly (***C5-trans*** is shown in red, ***C5C7−*** is shown in green, ***C5g-(s)*** is shown in blue, ***trans−trans*** is shown in purple, and ***C5g-(a)*** is shown in orange, respectively). Note that the *y*-axis range in panel a is shorter than that in panel b to facilitate the comparison between experimental and calculated vibrational transitions. Abbreviations: Am., amide; str., stretching; and wagg., wagging.

The calculated spectra of all conformers predict that the strongest experimental bands at 1782 and 1704 cm^{-1} correspond to the C═O stretching fundamental transitions. The latter band, known as amide I, originates from amide (peptide link) C═O stretching. Its position at 1704 cm^{-1} indicates that the observed spectrum is dominated by conformers with the free amide C═O group, implying no hydrogen bonding at this site. This allows us to conclude that the ***C5C7−*** and ***C5C7+*** conformers, which have a hydrogen-bonded amide C═O group, do not contribute significantly to the spectrum.

The question as to what extent planar (***C5-trans*** and ***trans−trans***) and nonplanar (***C5g-(s)*** and ***C5g-(a)***) conformers are populated can be assessed using spectral features in the so-called fingerprint frequency range below 1400 cm^{-1}. For example, the measured strong peak at 1393 cm^{-1} reflects the COH bending vibration of planar Gly-Gly conformers. In the case of nonplanar conformers, the calculated transition for this vibration is red-shifted and significantly reduced in intensity with respect to that of the planar counterparts. The normal-mode analysis also shows that two modes, including both CN and CO stretching vibrations observed at 1153 and 1120 cm^{-1}, are delocalized and are sensitive to the planarity of Gly-Gly. The intensities and the frequency spacing between the calculated transitions of these modes in the nonplanar conformers differ from the experiment. The same holds for the CC stretching vibrations. On the basis of these considerations, we can conclude that nonplanar conformers, such as ***C5g-(s)*** and ***C5g-(a)***, are not very important under our experimental conditions.

The remaining planar conformers ***C5-trans*** and ***trans−trans*** can be distinguished by other spectral features. For example, the calculated frequency of the NH_2 scissoring vibration for ***trans−trans*** (1638 cm^{-1}) is blue shifted with respect to the experiment (1620 cm^{-1}). Moreover, the CC stretching vibration has more delocalized character in the ***trans−trans*** conformer than in ***C5-trans***. Its calculated frequency for ***trans−trans*** (843 cm^{-1}) does not agree well with the experimental value of 863 cm^{-1}, whereas ***C5-trans*** (857 cm^{-1}) does. The NH_2 wagging (inversion) vibration involves a larger extent of NC and CC stretching in ***trans−trans***, resulting in a higher calculated frequency (895 cm^{-1}) that does not match the observed transition at 795 cm^{-1}. In summary, the calculated peak positions and intensities of the ***C5-trans*** conformer are in favorable agreement with the experimental spectrum whereas other conformers do not match to various degrees.

The predominance of the ***C5-trans*** conformer can be further verified by accounting for anharmonicity using the VPT2 approach (Figure 5). The VPT2 calculation for the ***C5-trans*** conformer accurately reproduces experimental band positions, yielding a mean absolute error (MAE) of as low as 6 cm^{-1}. The calculated overtone and combination bands (Figure 5) also eliminate some discrepancies between the scaled harmonic frequency and experimental spectra. For example, a relatively strong band observed at 1224 cm^{-1} was not predicted by the

DOI: 10.1021/acs.jpca.8b10881
J. Phys. Chem. A 2019, 123, 862−872

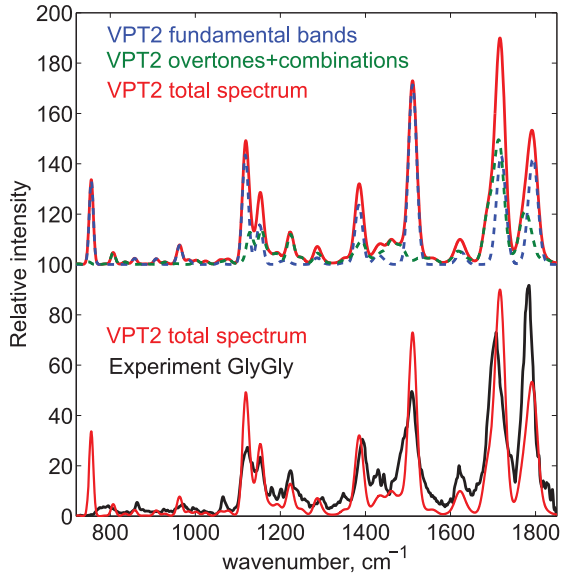

Figure 5. Anharmonic IR spectra for the ***C5-trans*** conformer calculated with VPT2, compared with the experimental IRMPD spectrum of Gly-Gly. The calculated spectra were convoluted with a Gaussian profile with a fwhm of 1.5% of the central frequency to match the experimental conditions.

harmonic frequency calculations. VPT2 predicts a strong band at this frequency corresponding to the overtone of the OH wagging + COH bending vibration. The reported high anharmonicity of the OH wagging vibration[50,63] supports this assignment.

The observation of a single conformer, ***C5-trans***, in our IRMPD spectroscopy study disagrees with theoretical abundances of the lowest-energy conformers (Figure 6a) calculated from the Gibbs free energy data at different temperatures. The temperature of laser-desorbed molecules is expected to be in the range of 350−500 K,[27] where the calculated population of the ***C5-trans*** conformer is less than 40%. To explain this seeming contradiction, conformational relaxation processes occurring in the supersonic jet need to be taken into account. Indeed, it is known that if the barriers to interconversion are low, then efficient conformational relaxations to the lowest-energy conformers take place during supersonic jet expansion.[52,64−68] Table 2 presents the calculated barrier heights for the possible relaxation pathways of Gly-Gly conformers. (See also Figure S4 in the Supporting Information.) The data were obtained using electronic energies ΔE_{el} and Gibbs free energies ΔG at 15 and 300 K. The barriers estimated from ΔG at 15 K are known to adequately describe relaxation for experimental conditions similar to ours[68] and therefore can be used to assess the likelihood of relaxation. As illustrated in Table 2, pathways I−VI have barriers lower than the critical value[52,54] of 800 cm^{-1}. This suggests that conformer relaxation via collisional cooling can occur along these pathways in our molecular beam. The barriers calculated at higher temperatures (e.g., at 300 K) were found to be much higher than those calculated at 15 K, with the single exception of ***sc-cis−trans*** → ***C5-trans*** relaxation. The cold environment of the supersonic jet is hence favorable to collisional relaxation, which would not take place at higher temperatures. We also note that the small negative value of ΔG(15 K) calculated for

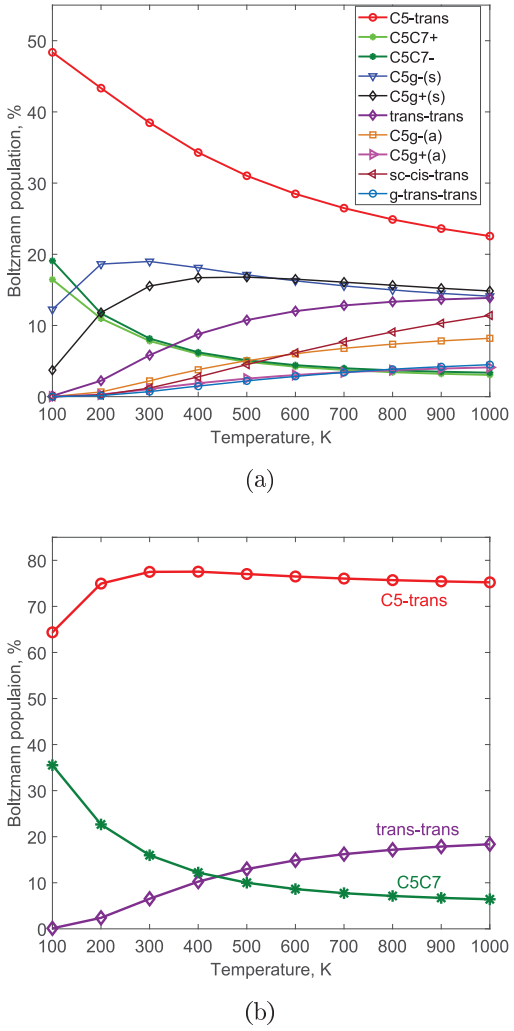

Figure 6. (a) Theoretical Boltzmann populations of the lowest-energy conformers of Gly-Gly, estimated from Gibbs free energies calculated at different temperatures. The Gibbs free energy data is taken from G4MP2 calculations that employed ωB97X-D geometries and frequencies. (b) Calculated Boltzmann populations that take into account the conformer relaxation processes in the argon jet. Conformers ***C5-trans***, ***trans−trans***, and ***C5C7±*** cannot undergo relaxation but gain population from other conformers as a result of relaxation processes I−VI (Table 2).

pathway I is most likely due to a calculation limitation affecting the intrinsic accuracy of the Gibbs free energy, which becomes apparent when structures with very similar geometries and energies are compared. According to the electronic energy calculation, the barrier for this pathway clearly exists, although it is very low (ΔE_{el} = 98 cm^{-1}).

Our calculations also suggest that the interconversion processes between lowest-energy conformers ***C5-trans***, ***trans−trans***, and ***C5C7±*** are not possible. (See pathways VII−IX in Table 2 and Figure S5 of the Supporting Information.) Such processes require several dihedral angles (relaxation coordinates) to be altered and involve high relaxation barriers (>800 cm^{-1}), which significantly reduces the probability of conversion.

Assuming complete relaxation[52,64,69−71] through pathways I−VI, the populations of the conformers that do not undergo relaxation (i.e., ***C5-trans***, ***trans−trans***, and ***C5C7±***) versus

DOI: 10.1021/acs.jpca.8b10881
J. Phys. Chem. A 2019, 123, 862−872

Table 2. Relaxation Barriers between the Lowest-Energy Conformers of Gly-Gly Calculated As the Differences between Energies of the Corresponding Conformers and Their Transition States, Based Either on the Electronic Energy Values, ΔE_{el} (G4MP2 Method), or on the Gibbs Free Energy Values at 15 and 300 K, ΔG(15 K) and ΔG(300 K)[a,b]

	relaxation pathway	relaxation coordinate	barrier to relaxation, cm^{-1}			energy difference
			ΔE_{el}	ΔG(15 K)	ΔG(300 K)	$\Delta(E_{el}$ + ZPE)
I.	*C5g-(s)* → *C5-trans*	ϕ_2	98	−27	410	90
II.	*C5g+(s)* → *C5-trans*	ϕ_2	94	19	327	179
III.	*C5g-(a)* → *C5g-(s)*	ψ_T	592	599	980	502
IV.	*C5g+(a)* → *C5g+(s)*	ψ_T	583	572	825	438
V.	*sc-cis−trans* → *C5-trans*	NH_2 inversion	699	402	374	755
VI.	*g-trans−trans* → *trans−trans*	ϕ_1	144	51	228	256
VII.	*C5C7−* → *int1*	θ_T, ψ_T, ϕ_2	2023	1857	1999	−1481
VIII.	*int1* → *C5-trans*	θ_T, ψ_T	3763	3466	3605	1494
IX.	*trans−trans*→ *sc-cis−trans*	ψ_1	913	911	1334	−347

[a]G4MP2 method, harmonic frequency, and hindered rotation analysis from ωB97X-D/6-311++G(d,p). [b]Note that ***int1*** is the intermediate conformer between ***C5C7−*** and ***C5-trans*** and is similar to ***C5-trans*** except for the θ_T dihedral that differs by 180°.

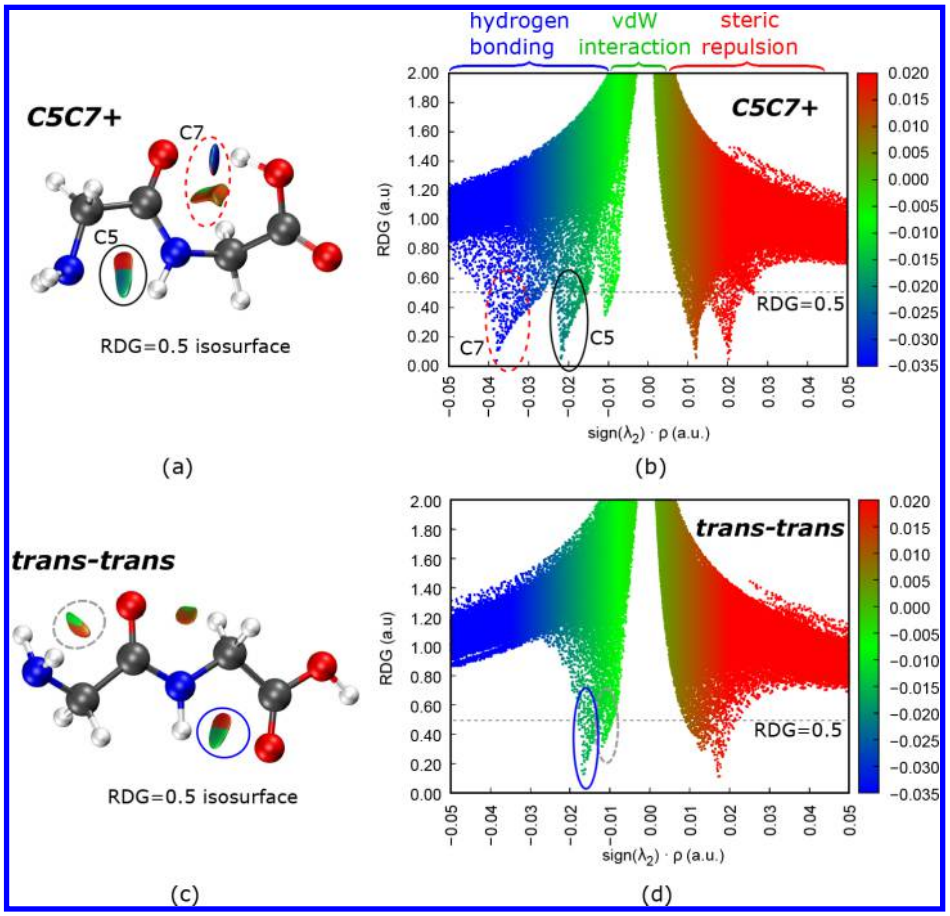

Figure 7. (a, c) The reduced density gradient (RDG) isosurface filled with a color map from $\text{sign}(\lambda_2)\rho$ for the ***C5C7*** conformer (a) and the ***trans−trans*** conformer (c) of Gly-Gly. (b, d) Corresponding scatter graph of RDG versus $\text{sign}(\lambda_2)\rho$ illustrating the type and strength of the attractive and repulsive noncovalent interactions that exist in the presented Gly-Gly structures. From the color map and the values of the electron density ρ observed when RDG is nearly zero, it can be seen that the OH···O hydrogen bonding interaction (C7) is stronger than the NH···N interaction (C5) in the ***C5C7*** structure. Moreover, the hydrogen bonding interactions in the ***trans−trans*** conformer are very weak, comparable to van der Waals attraction forces.

temperature are presented in Figure 6b. Note that because ***C5C7+*** and ***C5C7−*** are very similar in structure and energy, they are considered to be one structure, denoted as ***C5C7***. From this figure, it follows that the ***C5-trans*** structure is expected to be the most abundant under our experimental conditions. The predicted ratio among the populations of ***C5-trans***, ***trans−trans***, and ***C5C7*** conformers is 78:10:12 at 400 K. This result is in good agreement with our previous conclusion, drawn from the measured IRMPD spectrum, that ***C5-trans*** is the most abundant.

The three conformers that do not relax in the supersonic jet (Figure 6b) were observed in the recent rotational spectroscopy study of Gly-Gly,[26] though relative abundances of these conformers were not reported. The spectroscopic observation

DOI: 10.1021/acs.jpca.8b10881
J. Phys. Chem. A 2019, 123, 862−872

of presumably low-abundance ***C5C7−*** and ***trans−trans*** conformers (Figure 6b) is most probably related to the high resolution and sensitivity of the microwave (MW) spectroscopy technique. Although it is not possible to directly compare conformer abundances between the MW experiment and ours, one can expect the two methods to yield different populations of the conformers for two reasons. The laser ablation method (ps laser pulses, λ = 355 nm) employed in the MW study is known to result in an evaporated molecular ensemble with higher temperatures than the one achieved with the laser desorption method employed by us (ns pulses, λ = 1064 nm).[27] Moreover, the MW study used neon (15 bar) as a carrier gas, which is known to result in less efficient conformational relaxation[69,71] than when argon is used, as in the current measurements.

3.2. Hydrogen Bonding in Gly-Gly Conformers. There are some debates in the literature about the presence and importance of hydrogen bonding in glycine and alanine structures.[31,72−74] The functional groups of Gly-Gly structures are similar to glycine and alanine and can show similar weak noncovalent interactions. Therefore, we employed AIM (atoms in molecules) and NCI (noncovalent interactions) approaches to identify weak interactions in the Gly-Gly conformers.

Two types of relatively strong hydrogen bonding interactions were identified using the AIM approach. (See Figure S7 in the Supporting Information.) The first type corresponds to $H_2N\cdots HN$ hydrogen bonding (r(N···H) = 2.2 Å) that was found in most of the conformers with a cis configuration at the N-terminus. (See structures ***C5-trans***, ***C5g-(s)***, and ***C5C7+*** in Figure 3.) Such interaction leads to the formation of a ring involving five atoms, a so-called C5 interaction. If such a hydrogen bond is absent, then the cis configuration is less stable than the trans configuration. For example, the ***sc-cis−trans*** structure is less stable than the ***trans−trans*** structure (Table 1). Another strong interaction identified by the AIM approach corresponds to OH···O=C hydrogen bonding at the C-terminus (r(H···O) = 1.7 Å) that forms a seven-membered ring that is denoted by C7. This interaction stabilizes the ***C5C7+*** and ***C5C7−*** conformers. The relative distances between the BCPs and RCPs identified by the AIM analysis indicate that the C7 interaction is stronger than the C5 interaction.

Weaker hydrogen bonding interactions that could not be identified with the AIM method were found with the help of the NCI approach introduced by Jonson and co-workers.[33] Figure 7a,c illustrates the identified hydrogen bonding interactions (blue and green islands) for the ***C5C7+*** and ***trans−trans*** structures. Each interaction corresponds to a minimum in the plots of RDG versus sin(λ_2)ρ shown in Figure 7b,d. In such plots, the strength of noncovalent interactions is related to the sharpness of the minima and the values of ρ at the minima. For example, the NCI analysis clearly shows that hydrogen bonds in ***trans−trans*** are much weaker than those in ***C5C7+***.

The results of the NCI analysis applied to different Gly-Gly conformers are summarized in Table 3. (See also Figure S8 in the Supporting Information.) For each interaction found at the N- and C-termini, Table 3 lists the RDG values in different minima and the corresponding sin(λ_2)ρ values. These two numbers provide information on the type and strength of noncovalent interaction.[35] On the basis of the data from Table 3, several conclusions can be drawn.

Table 3. Minimum Values of RDG and the Corresponding sin(λ_2)ρ Values Associated with Different Attractive Interactions at the N- and C-Termini of Gly-Gly Structures[a]

	RDG(min)		sin(λ_2)ρ	
conformer	N-terminus	C-terminus	N-terminus	C-terminus
C5-trans	0	0.145	−0.0202	−0.0151
C5C7+	0	0	−0.0219	−0.038
C5g-(s)	0	0.137*	−0.022	−0.0148*
C5g+(s)	0	0.153*	−0.0216	−0.0147*
trans−trans	0.312	0.115	−0.012	−0.0165
g-trans−trans	0.081	0.081	−0.0165	−0.0165
sc-cis−trans	0.08	0.089	−0.0139	−0.0169

[a]The values denoted with * correspond to the weak CH···O=C interaction. Note that the interactions at the N- and C-termini of the ***g-trans−trans*** conformer have nearly identical strength, which hindered the discovery of the individual RDG and sin(λ_2)ρ values.

First, the planar conformers ordered by the increasing strength of their N-terminus hydrogen bonding attractive interaction are ***trans−trans*** < ***sc-cis−trans*** < ***g-trans−trans*** < ***C5-trans*** (Table 3). Interestingly, the interaction of the relatively stable ***trans−trans*** conformer is the weakest. (See also Figure 7c,d.) It is even weaker than CH···O=C interactions in the ***C5g±(s)*** structures and probably it does not contribute significantly to the stabilization of the ***trans−trans*** structure. On the other hand, the steric repulsion effects at the N-terminus of ***trans−trans*** are less pronounced than in the case of cis structures (Figure 7a,c.) Therefore, the reduced steric hindrance contributes to the relatively high stability of ***trans−trans***.

Second, the hydrogen bonding interactions at the C-terminus can have either weak CH···O=C character (***C5g±(s)***), weak C5 character (e.g., ***sc-cis−trans*** and ***trans−trans***), or strong C7 character (***C5C7+***). The NCI analysis showed that the formation of the C5 ring is associated with considerable steric repulsion effects that weaken the structural stabilization by the hydrogen bond. It was also found that the C5 interactions at the N- and C-termini show some competition due to sharing the same donor (amide NH group). For example, the C5 interaction at the N-terminus of the ***C5-trans*** conformer (ρ = 0.020) is slightly weaker than in the ***C5g±(s)*** structures (ρ = 0.022) that do not have donor sharing. Similarly, the hydrogen bond at the C-terminus of ***C5-trans*** (ρ = 0.015) is weaker than those in ***trans−trans*** and ***sc-cis−trans*** (ρ = 0.017).

Finally, as can be seen from Table 3, the ***sc-cis−trans*** conformer is associated with a weak interaction at the N-terminus, $H_2N\cdots HN$. It is almost twice as weak as the corresponding C5 interaction in the structurally similar ***C5-trans*** conformer, as observed by IRMPD-VUV spectroscopy. If we neglect the weak $H_2N\cdots HN$ interaction in ***sc-cis−trans***, then the energy stabilization due to the C5 interaction at the N-terminus of ***C5-trans*** can be estimated from the energy difference between the two conformers that is equal to 750 cm^{-1} (9 kJ/mol).

4. CONCLUSIONS

IRMPD-VUV spectroscopy of a cold molecular beam of laser-desorbed Gly-Gly revealed that the most dominant conformer of this dipeptide is ***C5-trans***, with the nearly planar cis−trans backbone structure stabilized by two C5 hydrogen bonding interactions. Interestingly, the contribution of the ***C5C7***

DOI: 10.1021/acs.jpca.8b10881
J. Phys. Chem. A 2019, 123, 862−872

conformer, stabilized by a strong C7 hydrogen bond, was found to be negligible in the measured spectrum. The explanation can be found in the rigidity of this structure that is associated with reduced entropy contributions[28,29] compared to more flexible structures such as ***C5-trans***. It is worth noting that Gibbs free energy calculations (Figure 6a) clearly capture the stabilization effect due to entropy, predicting that the ***C5-trans*** structure is more favorable than the ***C5C7*** structure at nonzero temperatures.

Conformational relaxation in the supersonic jet is another effect that was found to play an important role in the observation of the ***C5-trans*** conformer as the most dominant. The accurate determination of relaxation barriers between different conformers indicated that ***C5-trans*** can gain population from a number of low-energy conformers, making it the most abundant in a wide range of temperatures. It is worth noting that owing to extremely low barriers to interconversion (<200 cm^{-1}) between ***C5g±(s)*** and ***C5-trans***, the room-temperature gas-phase ensemble of Gly-Gly comprises a mixture of these structures that can easily interconvert. In the supersonic jet molecular beam, characterized by low temperatures and low-energy collisions, the equilibrium is shifted to the lowest-energy structure due to efficient collisional relaxation.[70,71]

The calculations also showed that two other conformers, ***C5C7*** and ***trans−trans***, observed recently by high-resolution MW spectroscopy,[26] remain populated in the jet with populations of about 10% each. Such fractions were unfortunately not revealed by IRMPD-VUV spectroscopy because of its limited resolution. If one is interested in studies of species with low relative abundances, then high-resolution spectroscopy methods are required. Such methods for neutral molecules are, however, limited to relatively small biomolecular building blocks[75] or require an aromatic moiety in the studied molecule.[14] The current study shows that the structure of the most stable conformers of peptides without an aromatic moiety can successfully be studied with IRMDP-VUV spectroscopy in combination with the jet-cooling method. As we observed, jet cooling is particularly efficient for conformational relaxation. The latter enables reducing the number of conformers populated, significantly simplifying the measured spectra. This is highly advantageous for spectroscopy of flexible peptides with a large degree of conformational heterogeneity.

The analysis of noncovalent interactions using the AIM and NCI approaches allowed us to assess the relative strength of hydrogen bonding in Gly-Gly conformers. It revealed two strong C5 and C7 interactions that stabilize the ***C5-trans*** and ***C5C7±*** conformers, while other hydrogen bonding interactions were found to be notably weaker. In the case of the ***trans−trans*** conformer, the particularly weak interaction at the N-terminus most probably does not play any significant role in the structure stabilization. By contrast, reduced steric hindrance, as revealed by the NCI analysis, contributes to its stability. Another plausible stabilization factor might be found in hyperconjugation effects,[31,73,74,76] which are outside the scope of this study. In general, the obtained insight into the weak intramolecular hydrogen bonding in Gly-Gly structures might be of interest to studies of the interplay between intra- and intermolecular interactions[6,77−79] as well as cooperative and long-range effects in peptide structures.[80−82]

■ ASSOCIATED CONTENT

Supporting Information

The Supporting Information is available free of charge on the ACS Publications website at DOI: 10.1021/acs.jpca.8b10881.

Energies of Gly-Gly conformers calculated using the G4MP2 and CBS-QB3 methods; calculated harmonic frequencies of OH and NH stretching vibrations of Gly-Gly conformers; bond lengths and angles of noncovalent interactions; comparison between the experimental IRMPD spectrum of Gly-Gly and the calculated spectra of conformers that were not presented in the article; performance assessment of DFT and MP2 methods for the prediction of Gly-Gly fundamental transitions; Gibbs free energies and Boltzmann populations obtained with the CBS-QB3 method; Gly-Gly conformer relaxation pathways; results of the AIM and NCI approaches as well as the relaxed PES scans studying the stability of the ***trans-g-(s)*** conformer (PDF)

■ AUTHOR INFORMATION

Corresponding Authors

*E-mail: a.rijs@science.ru.nl.

*E-mail: vitali.zhaunerchyk@physics.gu.se.

ORCID

Anouk M. Rijs: 0000-0002-7446-9907

Vitali Zhaunerchyk: 0000-0001-7302-7413

Notes

The authors declare no competing financial interest.

■ ACKNOWLEDGMENTS

We acknowledge the Swedish Research Council (VR), the Knut and Alice Wallenberg Foundation (Sweden), and NWO Physical Sciences (Netherlands) for financial support. The research leading to these results has received funding from LASERLAB-EUROPE (grant agreement no. 654148, European Union's Horizon 2020 Research and Innovation Programme). The authors greatly appreciate the skillful assistance of the staff at the FELIX laboratory. Calculations were performed with resources at the Chalmers Centre for Computational Science and Engineering (C3SE) provided by the Swedish National Infrastructure for Computing (SNIC). We also acknowledge NWO Physical Sciences (EW) for granting access to the supercomputer facilities at SurfSara (project no. MP-264-13).

■ REFERENCES

(1) Rijs, A.; Ohanessian, G.; Oomens, J.; Meijer, G.; von Helden, G.; Compagnon, I. Internal Proton Transfer Leading to Stable Zwitterionic Structures in a Neutral Isolated Peptide. *Angew. Chem., Int. Ed.* **2010**, *49*, 2332−2335.

(2) Schwing, K.; Gerhards, M. Investigations on Isolated Peptides by Combined IR/UV Spectroscopy in a Molecular Beam-Structure, Aggregation, Solvation and Molecular Recognition. *Int. Rev. Phys. Chem.* **2016**, *35*, 569−677.

(3) Chin, W.; Piuzzi, F.; Dimicoli, I.; Mons, M. Probing the Competition between Secondary Structures and Local Preferences in Gas Phase Isolated Peptide Backbones. *Phys. Chem. Chem. Phys.* **2006**, *8*, 1033−1048.

(4) de Vries, M. S.; Hobza, P. Gas-Phase Spectroscopy of Biomolecular Building Blocks. *Annu. Rev. Phys. Chem.* **2007**, *58*, 585−612.

DOI: 10.1021/acs.jpca.8b10881
J. Phys. Chem. A 2019, 123, 862−872

(5) Dean, J. C.; Buchanan, E. G.; Zwier, T. S. Mixed 14/16 Helices in the Gas Phase: Conformation-Specific Spectroscopy of Z(Gly)n, n = 1, 3, 5. *J. Am. Chem. Soc.* **2012**, *134*, 17186−17201.
(6) Nagornova, N. S.; Rizzo, T. R.; Boyarkin, O. V. Interplay of Intra- and Intermolecular H-Bonding in a Progressively Solvated Macrocyclic Peptide. *Science* **2012**, *336*, 320−323.
(7) Garand, E.; Kamrath, M. Z.; Jordan, P. A.; Wolk, A. B.; Leavitt, C. M.; McCoy, A. B.; Miller, S. J.; Johnson, M. A. Determination of Noncovalent Docking by Infrared Spectroscopy of Cold Gas-Phase Complexes. *Science* **2012**, *335*, 694−698.
(8) Ujma, J.; Kopysov, V.; Nagornova, N. S.; Migas, L. G.; Lizio, M. G.; Blanch, E. W.; MacPhee, C.; Boyarkin, O. V.; Barran, P. E. Initial Steps of Amyloidogenic Peptide Assembly Revealed by Cold Ion Spectroscopy. *Angew. Chem., Int. Ed.* **2018**, *57*, 213−217.
(9) Pace, C. N.; Shirley, B. A.; McNutt, M.; Gajiwala, K. Forces Contributing to the Conformational Stability of Proteins. *FASEB J.* **1996**, *10*, 75−83.
(10) Rose, G. D.; Fleming, P. J.; Banavar, J. R.; Maritan, A. A Backbonebased Theory of Protein Folding. *Proc. Natl. Acad. Sci. U. S. A.* **2006**, *103*, 16623−16633.
(11) DasGupta, D.; Varun, M.; Bhyravabhotla, J. A Component Analysis of the Free Energies of Folding of 35 proteins: A Consensus View on the Thermodynamics of Folding at the Molecular Level. *J. Comput. Chem.* **2017**, *38*, 2791−2801.
(12) Stauch, T.; et al. Spectroscopic Monitoring of Mechanical Forces during Protein Folding by using Molecular Force Probes. *ChemPhysChem* **2016**, *17*, 1486−1492.
(13) Rijs, A. M., Oomens, J., Eds. *Gas-Phase IR Spectroscopy and Structure of Biological Molecules*; Top. Curr. Chem., 2015; Vol. *364*; pp 1−406, and references therein.
(14) Rijs, A. M.; Oomens, J. In *Gas-Phase IR Spectroscopy and Structure of Biological Molecules*; Rijs, A. M., Oomens, J., Eds.; Springer International Publishing: Cham, 2015; pp 1−42.
(15) Compagnon, I.; Oomens, J.; Bakker, J.; Meijer, G.; von Helden, G. Vibrational Spectroscopy of a Non-Aromatic Amino Acid-based Model Peptide: Identification of the γ-turn Motif of the Peptide Backbone. *Phys. Chem. Chem. Phys.* **2005**, *7*, 13−15.
(16) Gloaguen, E.; Tardivel, B.; Mons, M. Gas phase Double-Resonance IR/UV Spectroscopy of an Alanine Dipeptide Analogue using a Non-Covalently Bound UVtag: Observation of a Folded Peptide Conformation in the Ac-Ala-NH2−Toluene Complex. *Struct. Chem.* **2016**, *27*, 225−230.
(17) Yatsyna, V.; Bakker, D.; Salen, P.; Feifel, R.; Rijs, A. M.; Zhaunerchyk, V. Infrared Action Spectroscopy of Low-Temperature Neutral Gas-Phase Molecules of Arbitrary Structure. *Phys. Rev. Lett.* **2016**, *117*, 118101.
(18) Leavitt, C. M.; DeBlase, A. F.; Johnson, C. J.; van Stipdonk, M.; McCoy, A. B.; Johnson, M. A. Hiding in Plain Sight: Unmasking the Diuse Spectral Signatures of the Protonated N-Terminus in Isolated Dipeptides Cooled in a Cryogenic Ion Trap. *J. Phys. Chem. Lett.* **2013**, *4*, 3450−3457.
(19) Wu, R.; McMahon, T. B. Protonation Sites and Conformations of Peptides of Glycine (Gly1−5H+) by IRMPD Spectroscopy. *J. Phys. Chem. B* **2009**, *113*, 8767−8775.
(20) Leavitt, C. M.; Wolk, A. B.; Kamrath, M. Z.; Garand, E.; Van Stipdonk, M. J.; Johnson, M. A. Characterizing the Intramolecular H-bond and Secondary Structure in Methylated GlyGlyH+ with H2 Predissociation Spectroscopy. *J. Am. Soc. Mass Spectrom.* **2011**, *22*, 1941.
(21) Fridgen, T. D.; MacAleese, L.; Maitre, P.; McMahon, T. B.; Boissel, P.; Lemaire, J. Infrared Spectra of Homogeneous and Heterogeneous Proton-Bound Dimers in the Gas Phase. *Phys. Chem. Chem. Phys.* **2005**, *7*, 2747−2755.
(22) Ung, H. U.; Moehlig, A. R.; Khodagholian, S.; Berden, G.; Oomens, J.; Morton, T. H. Proton-Bridge Motions in Amine Conjugate Acid Ions Having Intramolecular Hydrogen Bonds to Hydroxyl and Amine Groups. *J. Phys. Chem. A* **2013**, *117*, 1360−1369.
(23) Sanz, M. E.; Cabezas, C.; Mata, S.; Alonso, J. L. Rotational Spectrum of Tryptophan. *J. Chem. Phys.* **2014**, *140*, 204308.
(24) Pérez, C.; Mata, S.; Blanco, S.; López, J. C.; Alonso, J. L. Jet-Cooled Rotational Spectrum of Laser-Ablated Phenylalanine. *J. Phys. Chem. A* **2011**, *115*, 9653−9657.
(25) Pérez, C.; Mata, S.; Cabezas, C.; López, J. C.; Alonso, J. L. The Rotational Spectrum of Tyrosine. *J. Phys. Chem. A* **2015**, *119*, 3731−3735.
(26) Cabezas, C.; Varela, M.; Alonso, J. L. The Structure of the Elusive Simplest Dipeptide Gly-Gly. *Angew. Chem., Int. Ed.* **2017**, *56*, 6420−6425.
(27) Handschuh, M.; Nettesheim, S.; Zenobi, R. Is Infrared Laser-Induced Desorption a Thermal Process? The Case of Aniline. *J. Phys. Chem. B* **1999**, *103*, 1719−1726.
(28) Plowright, R. J.; Gloaguen, E.; Mons, M. Compact Folding of Isolated Four Residue Neutral Peptide Chains: HBonding Patterns and Entropy Effects. *ChemPhysChem* **2011**, *12*, 1889−1899.
(29) Shubert, V. A.; Baquero, E. E.; Clarkson, J. R.; III James, W. H.; Turk, J. A.; Hare, A. A.; Worrel, K.; Lipton, M. A.; Schoeld, D. P.; Jordan, K. D.; et al. Entropy-Driven Population Distributions in a Prototypical Molecule with Two Flexible Side Chains: O-(2-Acetamidoethyl)N-Acetyltyramine. *J. Chem. Phys.* **2007**, *127*, 234315.
(30) Koch, U.; Popelier, P. L. A. Characterization of C-H-O Hydrogen Bonds on the Basis of the Charge Density. *J. Phys. Chem.* **1995**, *99*, 9747−9754.
(31) Cormanich, R. A.; Ducati, L. C.; Rittner, R. Are Hydrogen Bonds Responsible for Glycine Conformational Preferences? *Chem. Phys.* **2011**, *387*, 85−91.
(32) Lane, J. R.; Contreras-García, J.; Piquemal, J.-P.; Miller, B. J.; Kjaergaard, H. G. Are Bond Critical Points Really Critical for Hydrogen Bonding? *J. Chem. Theory Comput.* **2013**, *9*, 3263−3266.
(33) Johnson, E. R.; Keinan, S.; MoriSánchez, P.; Contreras-García, J.; Cohen, A. J.; Yang, W. Revealing Noncovalent Interactions. *J. Am. Chem. Soc.* **2010**, *132*, 6498−6506.
(34) Contreras-García, J.; Yang, W.; Johnson, E. R. Analysis of Hydrogen-Bond Interaction Potentials from the Electron Density: Integration of Noncovalent Interaction Regions. *J. Phys. Chem. A* **2011**, *115*, 12983−12990.
(35) Lane, J. R.; Schrøder, S. D.; Saunders, G. C.; Kjaergaard, H. G. Intramolecular Hydrogen Bonding in Substituted Aminoalcohols. *J. Phys. Chem. A* **2016**, *120*, 6371−6378.
(36) Kung, A. H. Third-Harmonic Generation in a Pulsed Supersonic Jet of Xenon. *Opt. Lett.* **1983**, *8*, 24−26.
(37) Lockyer, M. P.; Vickerman, J. C. Single Photon Ionisation Mass Spectrometry Using Laser-Generated Vacuum Ultraviolet Photons. *Laser Chem.* **1997**, *17*, 139−159.
(38) Oomens, J.; Sartakov, B. G.; Meijer, G.; von Helden, G. Gas-Phase Infrared Multiple Photon Dissociation Spectroscopy of Mass-Selected Molecular Ions. *Int. J. Mass Spectrom.* **2006**, *254*, 1−19.
(39) Häber, T.; Jakobi, C. Random structure generator.
(40) Řezáč, J.; Hobza, P. Advanced Corrections of Hydrogen Bonding and Dispersion for Semiempirical Quantum Mechanical Methods. *J. Chem. Theory Comput.* **2012**, *8*, 141−151.
(41) Stewart, J. J. P. *MOPAC2009*; Stewart Computational Chemistry: Colorado Springs, CO, 2008; http://openmopac.net/.
(42) Frisch, M. J.; Trucks, G. W.; Schlegel, H. B.; Scuseria, G. E.; Robb, M. A.; Cheeseman, J. R.; Scalmani, G.; Barone, V.; Petersson, G. A.; Nakatsuji, H., et al. *Gaussian 16*, Revision A.03; Gaussian Inc.: Wallingford, CT, 2016.
(43) Kang, Y. K.; Park, H. S. Assessment of CCSD(T), MP2, DFT-D, CBS-QB3, and G4(MP2) Methods for Conformational Study of Alanine and Proline Dipeptides. *Chem. Phys. Lett.* **2014**, *600*, 112−117.
(44) Chai, J.-D.; Head-Gordon, M. LongRange Corrected Hybrid Density Functionals with Damped Atom-Atom Dispersion Corrections. *Phys. Chem. Chem. Phys.* **2008**, *10*, 6615−6620.
(45) Zhao, Y.; Truhlar, D. G. The M06 Suite of Density Functionals for Main Group Thermochemistry, Thermochemical Kinetics, Noncovalent Interactions, Excited states, and Transition Elements:

DOI: 10.1021/acs.jpca.8b10881
J. Phys. Chem. A 2019, 123, 862−872

Two New Functionals and Systematic Testing of Four M06-class Functionals and 12 Other Functionals. *Theor. Chem. Acc.* **2008**, *120*, 215−241.
(46) Grimme, S.; Ehrlich, S.; Goerigk, L. Effect of the Damping Function in Dispersion Corrected Density Functional Theory. *J. Comput. Chem.* **2011**, *32*, 1456−1465.
(47) Barone, V.; Cimino, P.; Stendardo, E. Development and Validation of the B3LYP/N07D Computational Model for Structural Parameter and Magnetic Tensors of Large Free Radicals. *J. Chem. Theory Comput.* **2008**, *4*, 751−764.
(48) Barone, V.; Biczysko, M.; Bloino, J. Fully Anharmonic IR and Raman Spectra of Medium-Size Molecular Systems: Accuracy and Interpretation. *Phys. Chem. Chem. Phys.* **2014**, *16*, 1759−1787 and references therein .
(49) Fornaro, T.; Biczysko, M.; Monti, S.; Barone, V. Dispersion Corrected DFT Approaches for Anharmonic Vibrational Frequency Calculations: Nucleobases and Their Dimers. *Phys. Chem. Chem. Phys.* **2014**, *16*, 10112−10128.
(50) Yatsyna, V.; Bakker, D. J.; Feifel, R.; Rijs, A. M.; Zhaunerchyk, V. Aminophenol Isomers Unraveled by Conformer Specific Far-IR Action Spectroscopy. *Phys. Chem. Chem. Phys.* **2016**, *18*, 6275−6283.
(51) Yatsyna, V.; Bakker, D. J.; Feifel, R.; Rijs, A. M.; Zhaunerchyk, V. Far-Infrared Amide IV-VI Spectroscopy of Isolated 2and 4-Methylacetanilide. *J. Chem. Phys.* **2016**, *145*, 104309.
(52) Godfrey, P. D.; Brown, R. D. Proportions of Species Observed in Jet Spectroscopy-Vibrational Energy Effects: Histamine Tautomers and Conformers. *J. Am. Chem. Soc.* **1998**, *120*, 10724−10732.
(53) Gloaguen, E.; de Courcy, B.; Piquemal, J. P.; Pilmé, J.; Parisel, O.; Pollet, R.; Biswal, H. S.; Piuzzi, F.; Tardivel, B.; Broquier, M.; et al. Gas-Phase Folding of a Two-Residue Model Peptide Chain: On the Importance of an Interplay between Experiment and Theory. *J. Am. Chem. Soc.* **2010**, *132*, 11860−11863.
(54) Gloaguen, E., Mons, M. In *Gas-Phase IR Spectroscopy and Structure of Biological Molecules*; Rijs, A. M., Oomens, J., Eds.; Springer International Publishing: Cham, 2015; pp 225−270.
(55) Montgomery, J. A.; Frisch, M. J.; Ochterski, J. W.; Petersson, G. A. A Complete Basis Set Model Chemistry. VII. Use of the Minimum Population Localization Method. *J. Chem. Phys.* **2000**, *112*, 6532−6542.
(56) Curtiss, L. A.; Redfern, P. C.; Raghavachari, K. Gaussian-4 Theory Using Reduced Order Perturbation Theory. *J. Chem. Phys.* **2007**, *127*, 124105.
(57) Bloino, J.; Biczysko, M.; Barone, V. General Perturbative Approach for Spectroscopy, Thermodynamics, and Kinetics: Methodological Background and Benchmark Studies. *J. Chem. Theory Comput.* **2012**, *8*, 1015−1036.
(58) Jaeqx, S.; Oomens, J.; Cimas, A.; Gaigeot, M.-P.; Rijs, A. M. Gas-Phase Peptide Structures Unraveled by Far-IR Spectroscopy: Combining IR-UV IonDip Experiments with Born-Oppenheimer Molecular Dynamics Simulations. *Angew. Chem., Int. Ed.* **2014**, *53*, 3663−3666.
(59) Ayala, P. Y.; Schlegel, H. B. Identification and Treatment of Internal Rotation in Normal Mode Vibrational Analysis. *J. Chem. Phys.* **1998**, *108*, 2314−2325.
(60) McClurg, R. B.; Flagan, R. C.; Goddard, W. A., III The Hindered Rotor Density of-States Interpolation Function. *J. Chem. Phys.* **1997**, *106*, 6675−6680.
(61) Peng, C.; Bernhard Schlegel, H. Combining Synchronous Transit and Quasi Newton Methods to Find Transition States. *Isr. J. Chem.* **1993**, *33*, 449−454.
(62) Lu, T.; Chen, F. Multiwfn: A Multifunctional Wavefunction Analyzer. *J. Comput. Chem.* **2012**, *33*, 580−592.
(63) Bakker, D. J.; Peters, A.; Yatsyna, V.; Zhaunerchyk, V.; Rijs, A. M. Far-Infrared Signatures of Hydrogen Bonding in Phenol Derivatives. *J. Phys. Chem. Lett.* **2016**, *7*, 1238−1243.
(64) Godfrey, P. D.; Brown, R. D.; Rodgers, F. M. The Missing Conformers of Glycine and Alanine: Relaxation in Seeded Supersonic Jets. *J. Mol. Struct.* **1996**, *376*, 65−81.
(65) Balabin, R. M. Conformational Equilibrium in Glycine: Experimental Jet-Cooled Raman Spectrum. *J. Phys. Chem. Lett.* **2010**, *1*, 20−23.
(66) Balabin, R. M. The Identification of the Two Missing Conformers of Gas-Phase Alanine: a Jet-Cooled Raman Spectroscopy Study. *Phys. Chem. Chem. Phys.* **2010**, *12*, 5980−5982.
(67) Valdes, H.; Reha, D.; Hobza, P. Structure of Isolated Tryptophyl-Glycine Dipeptide and Tryptophyl-Glycyl-Glycine Tripeptide: Ab Initio SCC-DFTB-D Molecular Dynamics Simulations and High-Level Correlated ab Initio Quantum Chemical Calculations. *J. Phys. Chem. B* **2006**, *110*, 6385−6396.
(68) Yang, B.; Liu, S.; Lin, Z. Computational Study on Single Molecular Spectroscopy of Tyrosin-Glycine, Tryptophane-Glycine and Glycine-Tryptophane. *Sci. Rep.* **2017**, *7*, 15869.
(69) Ruoff, R. S.; Klots, T. D.; Emilsson, T.; Gutowsky, H. S. Relaxation of Conformers and Isomers in Seeded Supersonic Jets of Inert Gases. *J. Chem. Phys.* **1990**, *93*, 3142−3150.
(70) Erlekam, U.; Frankowski, M.; von Helden, G.; Meijer, G. Cold Collisions Catalyse Conformational Conversion. *Phys. Chem. Chem. Phys.* **2007**, *9*, 3786−3789.
(71) Miller, T. F., III; Clary, D. C.; Meijer, A. J. H. M. Collision-Induced Conformational Changes in Glycine. *J. Chem. Phys.* **2005**, *122*, 244323.
(72) Wang, W.; Pu, X.; Zheng, W.; Wong, N. B.; Tian, A. Hyperconjugation Versus Intramolecular Hydrogen Bond: Origin of the Conformational Preference of Gaseous Glycine. *Chem. Phys. Lett.* **2003**, *370*, 147−153.
(73) Cormanich, R. A.; Ducati, L. C.; Tormena, C. F.; Rittner, R. A Theoretical Investigation of the Dictating Forces in Small Amino Acid Conformational Preferences: The Case of Glycine, Sarcosine and N,N-Dimethylglycine. *Chem. Phys.* **2013**, *421*, 32−38.
(74) Cormanich, R. A.; Ducati, L. C.; Rittner, R. The Lack of Intramolecular Hydrogen Bonding and the Side Chain Effect in Alanine Conformers. *J. Mol. Struct.* **2012**, *1014*, 12−16.
(75) Alonso, J. L.; López, J. C. In *Gas-Phase IR Spectroscopy and Structure of Biological Molecules*; Rijs, A. M., Oomens, J., Eds.; Springer International Publishing: Cham, 2015; pp 335−401.
(76) Wathen, B.; Pratt, D. A.; Jia, Z. Hyperconjugation Contributes to the Bimodal Distribution of Glycine Conformations Observed in Protein Three-Dimensional Structures. *ChemBioChem* **2011**, *12*, 1674−1677.
(77) Marsh, B. M.; Duffy, E. M.; Soukup, M. T.; Zhou, J.; Garand, E. Intramolecular Hydrogen Bonding Motifs in Deprotonated Glycine Peptides by Cryogenic Ion Infrared Spectroscopy. *J. Phys. Chem. A* **2014**, *118*, 3906−3912.
(78) Awada, H.; Grison, C. M.; CharnayPouget, F.; Baltaze, J.-P.; Brisset, F.; Guillot, R.; Robin, S.; Hachem, A.; Jaber, N.; Naoufal, D.; et al. Conformational Effects through Hydrogen Bonding in a Constrained γ-Peptide Template: From Intraresidue Seven-Membered Rings to a Gel-Forming Sheet Structure. *J. Org. Chem.* **2017**, *82*, 4819−4828.
(79) Bakker, D. J.; Dey, A.; Tabor, D. P.; Ong, Q.; Mahé, J.; Gaigeot, M.-P.; Sibert, E. L.; Rijs, A. M. Fingerprints of Inter-and Intramolecular Hydrogen Bonding in Saligenin-Water Clusters Revealed by Mid- and Far-infrared spectroscopy. *Phys. Chem. Chem. Phys.* **2017**, *19*, 20343−20356.
(80) Maekawa, H.; Ballano, G.; Toniolo, C.; Ge, N.-H. Linear and Two-Dimensional Infrared Spectroscopic Study of the Amide I and II Modes in Fully Extended Peptide Chains. *J. Phys. Chem. B* **2011**, *115*, 5168−5182.
(81) Horváth, V.; Varga, Z.; Kovács, A. LongRange Effects in Oligopeptides. A Theoretical Study of the β-Sheet Structure of Glyn (n = 2−10). *J. Phys. Chem. A* **2004**, *108*, 6869−6873.
(82) Wieczorek, R.; Dannenberg, J. J. Hydrogen-Bond Cooperativity, Vibrational Coupling, and Dependence of Helix Stability on Changes in Amino Acid Sequence in Small 310-Helical Peptides. A Density Functional Theory Study. *J. Am. Chem. Soc.* **2003**, *125*, 14065−14071.

DOI: 10.1021/acs.jpca.8b10881
J. Phys. Chem. A 2019, 123, 862−872